CHAPTER - 6

GEOCHEMISTRY

6.1 Introduction

The word "geochemistry" is constituted from two words; "geo" (the Earth) and "chemistry" (a branch of science that deals with chemical transformation). To understand and quantify the chemical composition and structural properties of rocks, a petrologist needs to look for the chemistry of the rock, termed geochemistry. The Earth's crust is primarily composed of igneous rocks, which are primary rocks derived from magmas. Major and trace element chemistry can broadly define the nature of metamorphic rock suites. Most metamorphic rocks are made up of silicates, aggregates of one or more minerals,and naturally occurring inorganic chemical compounds. The present chapter embodies the geochemical characteristics of the pelitic granulites, garnet-biotite gneisses and amphibolites from the study area. It provides a hypothesized model for these rocks' evolutionary history. Geochemical characterization of metamorphic rocks is required to understand the tectonic evolution of the rocks in the studied region. The goal of the present study is to

- Whether the high-grade gneisses and granulites are magmatic/orthometamorphic or parametamorphic,
- Whether magmatic signatures have been preserved and, if so, what was the nature of the source magma or tectonic environment for magma generation,
- Whether there is an overall signature of depletion of large-ion lithophile elements (LILE) and an enhancement of K/Rb ratios, and
- To what extent are different granulites chemically comparable to the Indian granulites province's similar suites

6.2 Major oxides Geochemistry

The most abundant oxides in metamorphic rocks, which are dealt with in order of increasing atomic numbers, are the oxides of sodium (Na_2O), magnesium (MgO), aluminium (Al_2O_3), silicon (SiO_2), phosphorus (P_2O_5), potassium (K_2O), calcium (CaO), titanium (TiO_2), manganese (MnO) and iron (Fe, both ferric Fe_2O_3 and ferrous FeO). They are mostly used for rock classification and the construction of variation diagrams. Major elements present in an amount on the Earth's crust of more than 1wt % and trace elements are less than 1 wt % because the behaviour of the major oxides in magmas can be manifested in terms of differentiation index. Likewise, trace elements behave similarly to major elements because they substitute for major elements. Based on quantitative measurements and patterns of geochemical variations, geochemistry is the most effective tool for distinguishing the protolith of metamorphic rocks, identifying involved magmatic processes and the nature of melt, and determining the tectonothermal environment. With many discrimination diagrams employed in the literature, it is fascinating to decide whether the metamorphic rocks' protoliths are of sedimentary or igneous origin. In the present context, the discrimination function (DF) (Shaw, 1972) is derived by:

$$\mathbf{DF = 10.44 - 0.21SiO_2 - 0.32Fe_2O_3(totalFe) - 0.98MgO + 0.55CaO + 1.46Na_2O + 0.54K_2O}$$

6.3 Trace Element Geochemistry

Trace element geochemistry has been appreciated for establishing or determining the rock's evolution and is also used for recognizing its depositional environment. The comparative abundances of trace elements are broadly recognized in the evolutionary process because they are sensitive to partial melting, crystal fractionation, and source composition. The trace element proportion of the melt depends on the parent material, the melting process, the remaining crystal phases after removing the melt, any differentiation before complete

crystallization and any possible interaction with rocks, melts or fluids (Hanson, 1989). The trace elements would provide better tools for understanding the geochemical process than the major oxides. The concentration of these elements (Rb, Sr, Nb, Zr, Ba, Cs, Hf, Ta, Pb, etc.) in rock is less than 0.1% and is expressed in parts per million (ppm). They are used to study elemental distribution in crystal-melt equilibria. Trace elements that have priority in the mineral phase are described as compatible. In contrast, elements that have a melting preference are said to be incompatible (Pearce, 1983). Based on the charge-size ratio or ionic potential, incompatible elements are categorized into high field strength (HFS) elements (Sc, Ta, Y, U, Nb, Pb, Hf) and LILE (Cs, Rb, Ba).

6.4 Rare Earth Elements Geochemistry

The geochemical behaviour of rare earth elements (REE) changes gradually from La to Lu. The REE contents of igneous rocks offer significant evidence about the magma source, the degree of partial melting of that source, the degree of crustal contamination, and the quantity of crystal fractionation during magma evolution. REEs are typically immobile following igneous alteration and low-grade metamorphism (Hanson, 1989). REEs patterns help to understand the magmatic bodies' petrogenesis process and tectonic discriminate setting (Pearce, 1983).

REE are a group of 15 (trace) elements with an atomic number from 57 (La) to 71 (Lu); 14 of these elements (except Promethium-Pm) occur naturally. For convenience, the REEs are divided into two sub-groups: (i) La to Smare denoted as the light rare earth elements (LREE) and (ii) Gd to Lu are recognized as the heavy rare earth elements (HREE). However, middle rare earth elements (MREE) are applied to the elements from about Sm to Ho (Henderson, 1984). In nature, all of the rare earth elements exhibit a 3+ oxidation state (trivalent), except Ce^{4+} (oxidized) and Eu^{2+} (reduced) under most geological conditions.

6.5 Analytical techniques

In the present study, eighteen representative samples from the Mauranipur and Babina greenstone belts of BuC were chemically analyzed for the major, trace, and REEs. The geochemical data of various rocks are given in Tables 6.1-6.4. To avoid contamination, representative samples were selected from the unweathered surface and crushed using a jaw crusher, pulverization mill, an agate mortar. XRF carried out whole rock major elemental analyses, and trace REE analysis was carried out by ICP-MS, the details of which are given below. Various variation diagrams and ratio correlations have been utilized to analyze the behaviour of major, trace, and REE elements in various rocks.

6.5.1 XRF and ICP-MS

For major oxide, trace, and REE analysis, XRF (X-Ray Fluorescence) and ICP-MS (Inductive Coupled Plasma-Mass Spectrometry) were used. These were carried out at the BirbalSahni Institute of Palaeosciences (BSIP), Lucknow, India. The pressed powder method was used to make the samples, with boric acid as a binder (boric acid: sample ratio, 2:3). Major oxides were analyzed by XRF using a wavelength dispersive (WD-XRF AXIOS MAX) machine with power of 4KW, 60kV-160mA analytical, on a pressed powder pellet machine using 'kameyo' at pressure of 15-20 tons with a 4mm pallet thickness. REEs were analyzed by ICP-MS (Make: Agilent, Model: ICP-MS 7700). All of the solutions were made with ultrapure water (18.2 MX). All the samples were digested by taking 30 mg (300 mesh) sediment powder and using supra pure acid (HF, $HClO_4$, HNO_3). Four solutions (10, 40, 100, 200, and 300 ppb for all elements) were prepared by 71A and 71B multi-element calibration standard solutions (Inorganic Ventures) as external calibration. The data set will be less than 5% off with the correct calibration curve.

6.6 Pelitic granulites

6.6.1 Major oxides

Geochemical analysis of pelitic granulites reveals much about the protoliths and their geodynamic settings. Table 6.1& 6.2 shows the major, trace, and REE values of the pelitic granulites studied, with loss of ignition ranging from 0.27 to 0.62 for Grt-Opx-Bt-Sill, from 0.27-0.54 for Grt-Bt-Sill, and 0.49 to 0.55 for Grt-Opx-Crd-Bt-Sill.

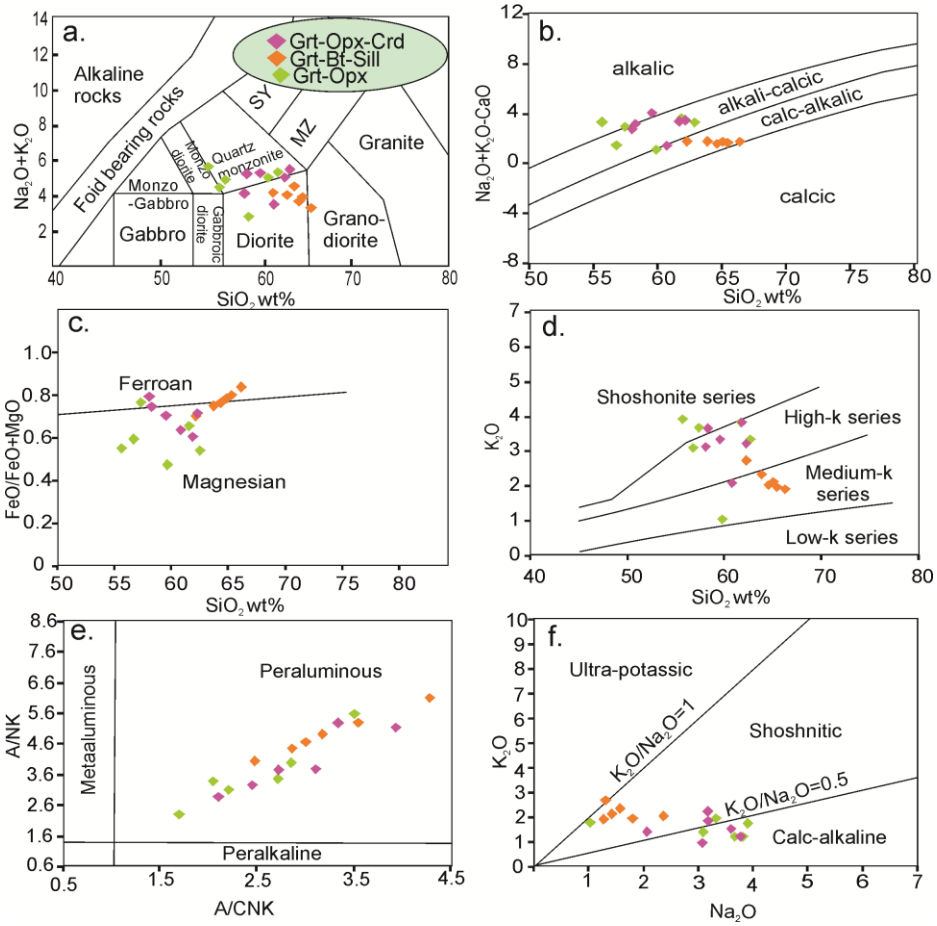

Figure 6.1 Chemical classification diagrams using major element composition of the studied rocks. (a) Total alkali versus silica (TAS) diagram for plutonic rocks after Middlemost (1994). (b) Calcic to alkali-calcic via calc-alkaline nature of pelitic granulites. (c) Granitoid classification scheme by Frost et al. (2001) revealing magnesian to ferroan. (d) K_2O versus SiO_2 plot after Peccerillo and Taylor (1976). (e) A/CNK versus A/NK diagram. (f) Na_2O versus K_2O diagram (after Turner et al., 1996).

The total alkali-silica (TAS: Middlemost, 1994) diagrams of pelitic granulites (Fig. 6.1a) show diorite, granodiorite, and quartz–monzonite fields, showing that the protolith of pelitic granulites came from a variety of sedimentary provenances. Furthermore, the plot of (SiO_2) vs (Na_2O + K_2O–CaO) demonstrates the transition from calc-alkalic to alkali-calcic

nature (Fig. 6.1b). Most samples are magnesian, while some are ferroan (Fig. 6.1c). The SiO_2versus K_2O figure (Fig. 6.1d) also shows that pelitic granulites dominate the high–K and medium–K calc-alkaline series. All pelitic granulite samples are peraluminous (Fig. 6.1e). The shoshonitic and calc-alkaline compositions are represented by the Na_2O against the K_2O plot (Fig. 6.1f).

6.6.2 Trace and REEs

The primitive mantle normalized multi-elemental spider diagram is widely used to determine the nature of trace elements in pelitic granulites and constrain their source regions. Incompatible elements (Rb, Ba, Y, Zr, and Th) predominate in trace elements, and compatible elements (Cr, Ni, Cu, and Co) are scarce. The wide range of LFSE elements could be attributed to the varied metamorphic conditions and degrees of mobility during protolith transformation.

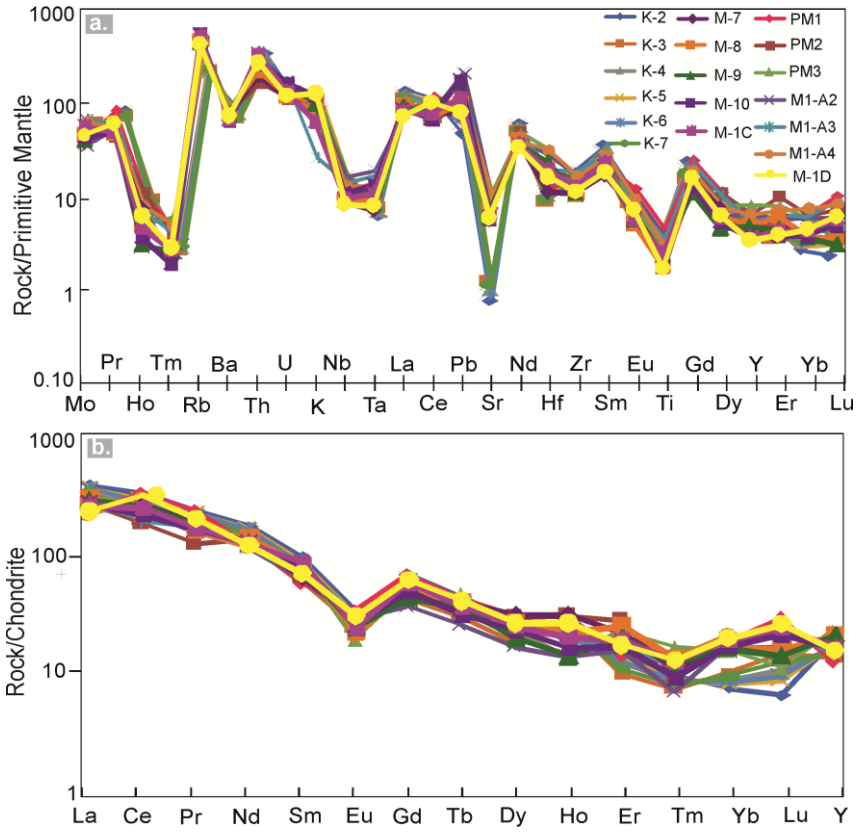

Figure 6.2 (a) Primitive mantle normalized multi-element spider diagram of pelitic granulites. Normalized values are after Sun and McDonough (1989). (b) Chondrite normalized rare earth element plot. Normalized values are after Sun and McDonough (1989).

In the primitive-mantle-normalized trace-element spider diagram, positive anomalies are detected for Ba, K, Pb, Nd, Sm, Gd, and Y, but significant negative anomalies are detected for high field strength elements (HFSEs) such as Nb, Ta, and Ti (Fig. 6.2a), indicating a characteristic feature of subduction orogeny. A decrease in Nb and Ti concentrations confirmed an island arc setting. The rare earth element (REE) patterns normalized with chondrite for pelitic granulites are used to define the behaviour of REEs in the studied rocks and to understand their source compositions (Fig. 6.2b).

All samples have positive Eu anomalies in the chondrite-normalized REE patterns (Fig. 6.2b). The sub-parallel REE patterns show that a phase of compositional fluctuation dominated crystal fractionation. The pelitic granulites have a high fractionated light REE pattern with a low and unfractionated heavy REE (HREE) pattern; the pattern appears to be flat, and Eu (Eu_N/Eu^* = 0.30-0.59) has negative anomalies. Except for Ho, Tm, and Lu, the variance in abundance of these elements is relatively small. The $(La/Lu)_N$ ratios in these samples range from 7.95 to 56.85, indicating a high degree of fractionation.

6.6.3 Discussion

Based on the normalized trace and rare-earth element (REE) patterns and discrimination diagrams, we have concluded the nature of the parental rock and tectonic settings of studied pelitic granulites during their formation. Geochemical attributes added with field observations and discrimination diagrams appear to be helpful for the characterization of pelitic granulites. According to the geochemical study, pelitic granulites are formed by the deposition of felsic sediments along a convergent margin and are then metamorphosed. The time since sedimentation and their source locality with the metamorphism after the deposition play a vital role in uncovering the tectonic history. The geochemical data of pelitic granulites show their unusual composition because they do not correspond to any normal igneous or sedimentary rocks. The minerals of the pelitic

granulites' total composition suggest that they were derived from argillaceous parent rocks. However, no undesirable sedimentary structures have survived due to the rocks' recrystallization and reconstitution. Generally, the element's movement is reported between the coexisting mineral phases, so few elements tend to migrate from the crystal phase to the melt phase during metamorphism. Low TiO_2 and high Al, K, and Si content reveal that granitic-rich sediments dominated the pelitic provenance. Pelitic granulites contain a good amount of Ba and Rb, as the feldspar is an essential mineral for hosting Ba and Rb in terrigenous sedimentary rocks. Moreover, the analyzed geochemical data indicate that pelitic granulites are probably redeposited and metamorphosed products of weathered Archean crusts.

6.6.3.a The Nature of the Original Sediments

The data of pelitic granulites were plotted on a discrimination diagram of log (Fe_2O_3/K_2O) versus log (SiO_2/Al_2O_3) after Herron (1988), to identify the lithological properties of the original sediment (Fig.6.3a). It represents a separate collection of data plots in the shale field, with one sample on the shale and Fe-shale field boundary. The P_2O_5/TiO_2vs MgO/CaO (after Werner 1987) figure reveals that the rocks are of recycled sedimentary origin (Fig.6.3b). There are no definitive criteria for recognizing the characteristics of the primitive magmatic material of the reworked sediments; however, Pinto et al. (2004) produced some discrimination plots. During sedimentary processes, elements with low mobility are employed to discriminate between distinct igneous source rocks. The Chemical Index of Alteration (CIA) vs Index of Compositional Variability (ICV) discrimination diagram also shows the recycled metasediments, as the protolith of the pelitic granulites themselves originated from an andesitic source (Fig.6.3c) (Potter et al., 2005). The data point cluster on the SiO_2vs log (Na_2O/K_2O) diagram (Roser and Korsch 1988) for the protolith of

pelitic granulites suggests that the depositional environment was an active continental margin (ACM) (Fig.6.3d).

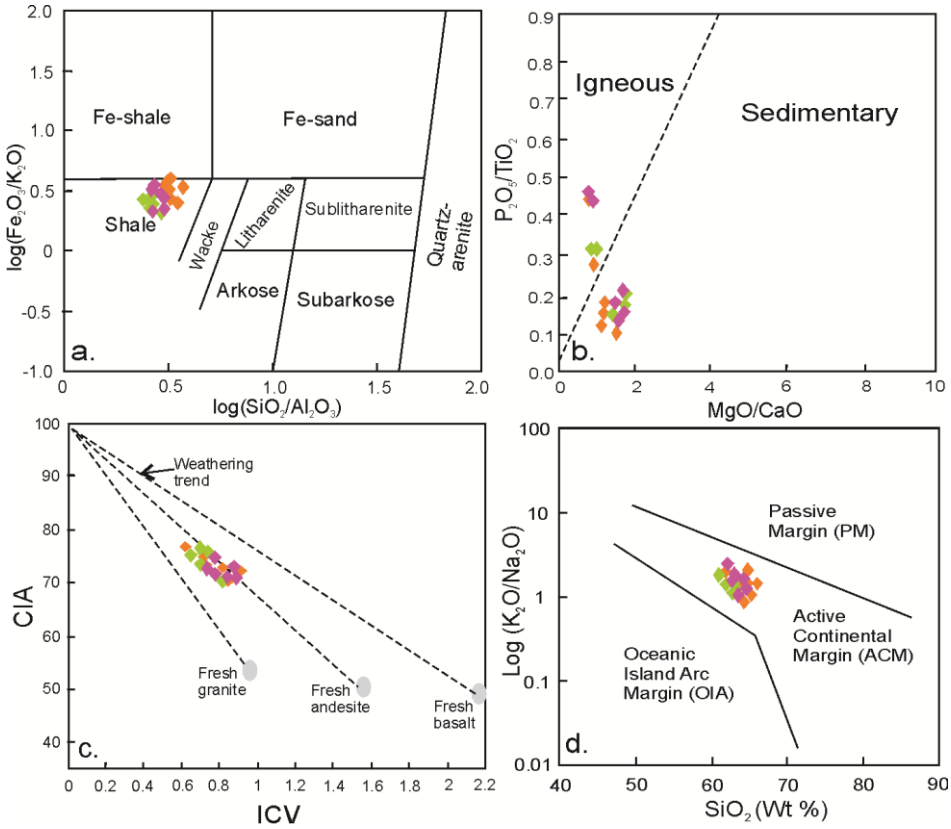

Figure 6.3 (a) $log(SiO_2/Al_2O_3)$ vs $log(Fe_2O_3/K_2O)$ plot after Herron (1988) (b) The MgO/CaO vs P_2O_5/TiO_2 diagram after Werner (1987) (c) CIA versus ICV diagram of Potter et al. (2005) (d) SiO_2 vs. $log(K_2O/Na_2O)$ diagram after Roser and Korsch (1988).

6.6.3.b Provenance and tectonic setting

The provenance of the pelitic granulites is established with the help of discrimination function analysis, in which the major oxides and trace elements have been utilized (Roser and Korsch 1988). This discrimination function analysis differentiates four provenance fields: mafic igneous, intermediate igneous, felsic igneous, and quartzose sedimentary or recycled provenance. The pelitic granulites acquire the domain of felsic igneous provenance when plotted in the discrimination function diagram (Fig. 6.4a). The TiO_2 versus Zr plot confirms this as all the pelitic granulite samples are again plotted in the felsic igneous rocks field (Fig. 6.4b). The trace-element data is utilized to construct tectonic discrimination diagrams that

highlight the parental rock's properties and the type of tectonism. The $(Y/Nb)_N$ vs $(Th/Nb)_N$diagram has been used to differentiate between oceanic islands, continental crust, and convergent margin rocks, with all samples falling into the convergent margin rocks field (Fig.6.4c). The Zr against Nb/Zr curve (Fig.6.4d) suggests that the protolith of pelitic granulites was exposed to a subduction-related tectonic setting.

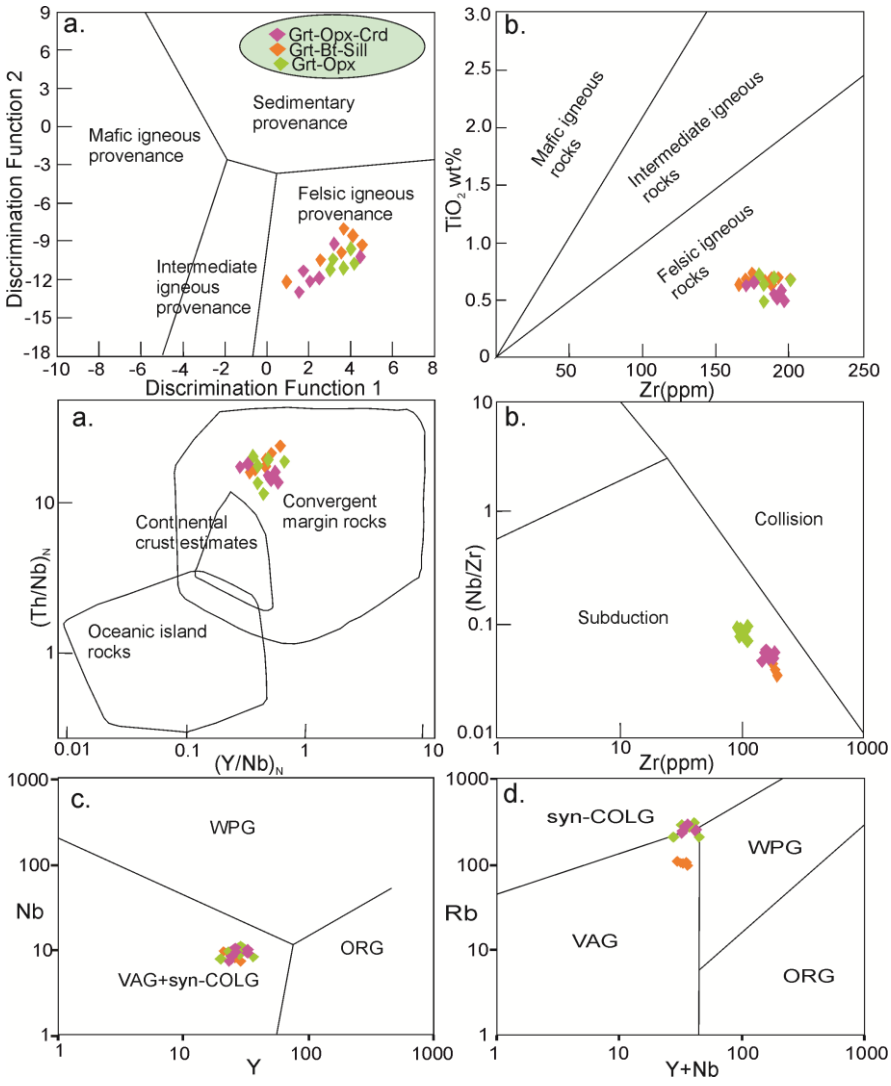

Figure 6.4 (a) Major element Discriminant Function diagram for provenance after Murali et al. (1988), where Discriminant Function 1 = (−1.773 TiO_2) + (0.607 Al_2O_3) + (0.760 Fe_2O_3) + (−1.500 MgO) + (0.616 CaO) + (0.509 Na_2O) + (−1.224 K_2O) + (−9.090); Discriminant Function 2 = (0.445 TiO_2) + (0.070 Al_2O_3) + (−0.250 Fe_2O_3) + (−1.142 MgO) + (0.438 CaO) + (1.475 Na_2O) + (−1.426 K_2O) + (-6.861). (b) TiO_2–Zr plot of aluminium samples after Hayashi et al. (1977). (c) (Y/Nb)N versus (Th/Nb)N diagram after Moreno et al. (2014), (d) Zr versus Nb/Zr plot after Thieblemont and Tegyey (1994), (e) Y vs Nb tectonic discrimination diagram. (f) Y+Nb vs Rb tectonic discrimination plot. Syn-COLG: syn-collisional granite; WPG: within plate granite; VAG: volcanic arc granite; ORG: ocean ridge granite (after Pearce et al.1984).

The Y vs Nb plot suggests that the pelitic granulite protolith came from volcanic arc granite (VAG) and a syn-collisional tectonic environment (Fig. 6.4e), whereas the Y+NbvsRb plot verifies that the protolith came from VAG (Fig. 6.4f). The enrichment of K, Th, U, Pb, and HREE in the investigated rocks, as well as the depletion of Nb, Sr, and Ti in the protolith, are both linked to the mid-upper crust or subduction-related formation of their protolith (Rudnick and Gao, 2004).

6.7 Garnet-Biotite gneisses

6.7.1 Major oxides

The results of the geochemical analysis for the Grt-Bt gneisses are presented in table 4. The Grt-Bt gneisses are compositionally variable in major oxides as; SiO_2 (57.64–77.83 wt%), Al_2O_3 (7.46–16.31 wt%), MgO (0.47–8.02 wt%), FeO (2.61–13.91 wt%), K_2O (0.99–3.13 wt%), and also contains lesser amounts of TiO_2 (0.62–1.66 wt%), CaO (1.80–3.51 wt%), Na_2O (1.03–3.26 wt%) and P_2O_5 (0.14–0.65 wt%). Samples show considerable variation in the K_2O/Na_2O ratios of 0.78–1.55, suggesting its potassium-rich character. The combined alkali (K_2O+Na_2O) wt% is 2.03–6.11. The $Al_2O_3/(CaO+ Na_2O + K_2O)$ ratio ranges between 1.00 and 2.34. The bivariate diagrams (Fig.6.5) plotted for the major oxides of Grt-Bt gneisses. Major oxides are plotted against the SiO_2 wt% to reveal magmatic evolution through elemental partitioning. A negative correlation is found between SiO_2 with MgO, TiO_2, FeO, CaO, MnO, and Al_2O_3, while a positive correlation between SiO_2 with Na_2O and K_2O is experienced. During post-crystallization processes, high mobility elements represent scattered data plots of MgO with Na_2O and K_2O. The decrease in FeO and TiO_2 with increasing SiO_2 and the robust negative anomaly of Nb and Ti recommends fractionation of Fe-Ti oxides for all the mafic granulite samples. The Grt-Bt gneisses are plotted on the total alkali versus silica (TAS) diagram (Fig.6.6a), as well as the K_2O vs SiO_2 diagram (Fig.6.6b), which indicates the calc-alkaline series.

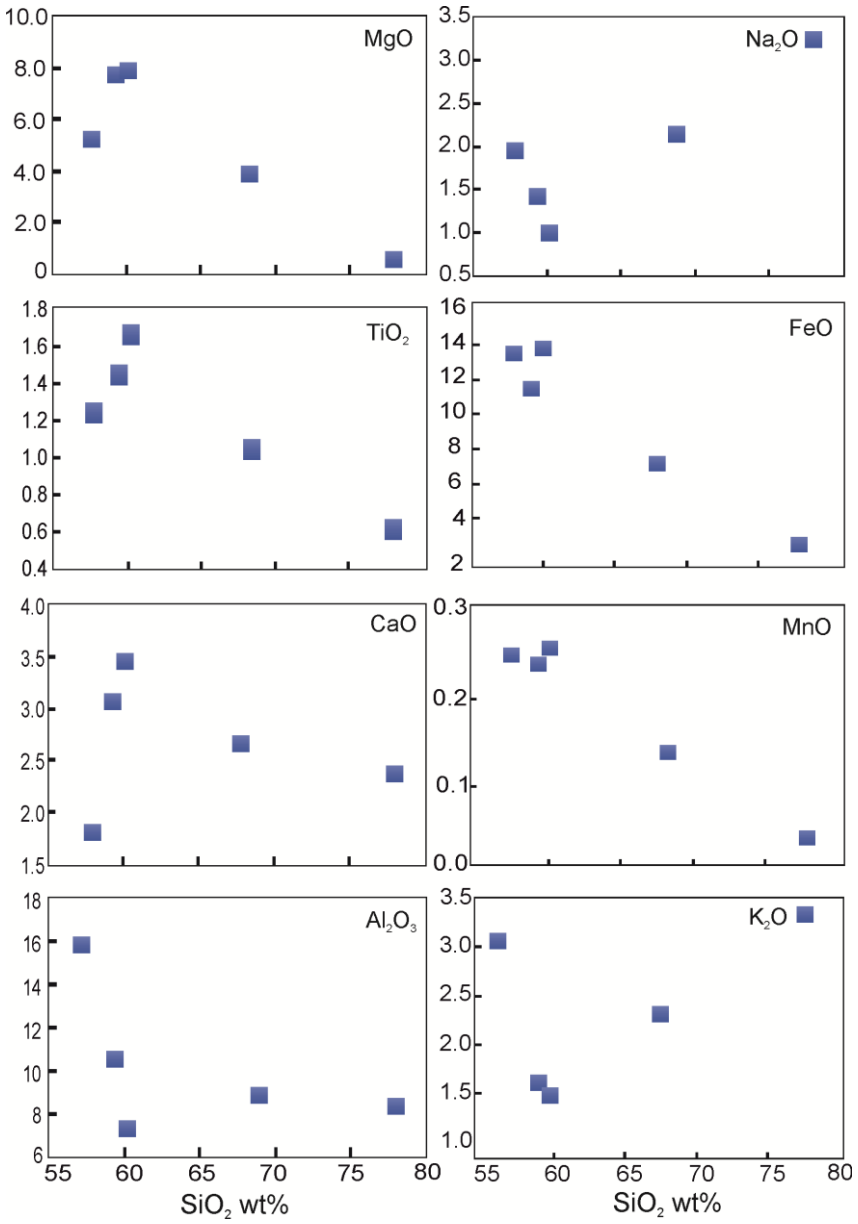

Figure 6.5 Fenner's binary diagram showing moderate to strong fractionation trends for selected major elements oxide versus $SiO_2$of garnet-biotite gneisses.

6.7.2 Trace and REEs

The primitive mantle normalized spider diagram of Grt-Bt gneisses reveals depletion of Mo, Ho, Tm, Ba, K, Nb, Sr, Hf, Ti, and an abundance of Rb, Th, U, La, Ce, Nd, and Gd (Fig.6.6c). The REE chondrite normalized patterns (Fig.6.6d) show enriched LREE and depletion in HREE with high to moderate $(La/Yb)_N$. The Grt-Bt gneisses show slight negative Eu anomalies ($Eu/Eu* = 0.7-1.0$). The Y-content (20.7−38.16) is high for all samples.

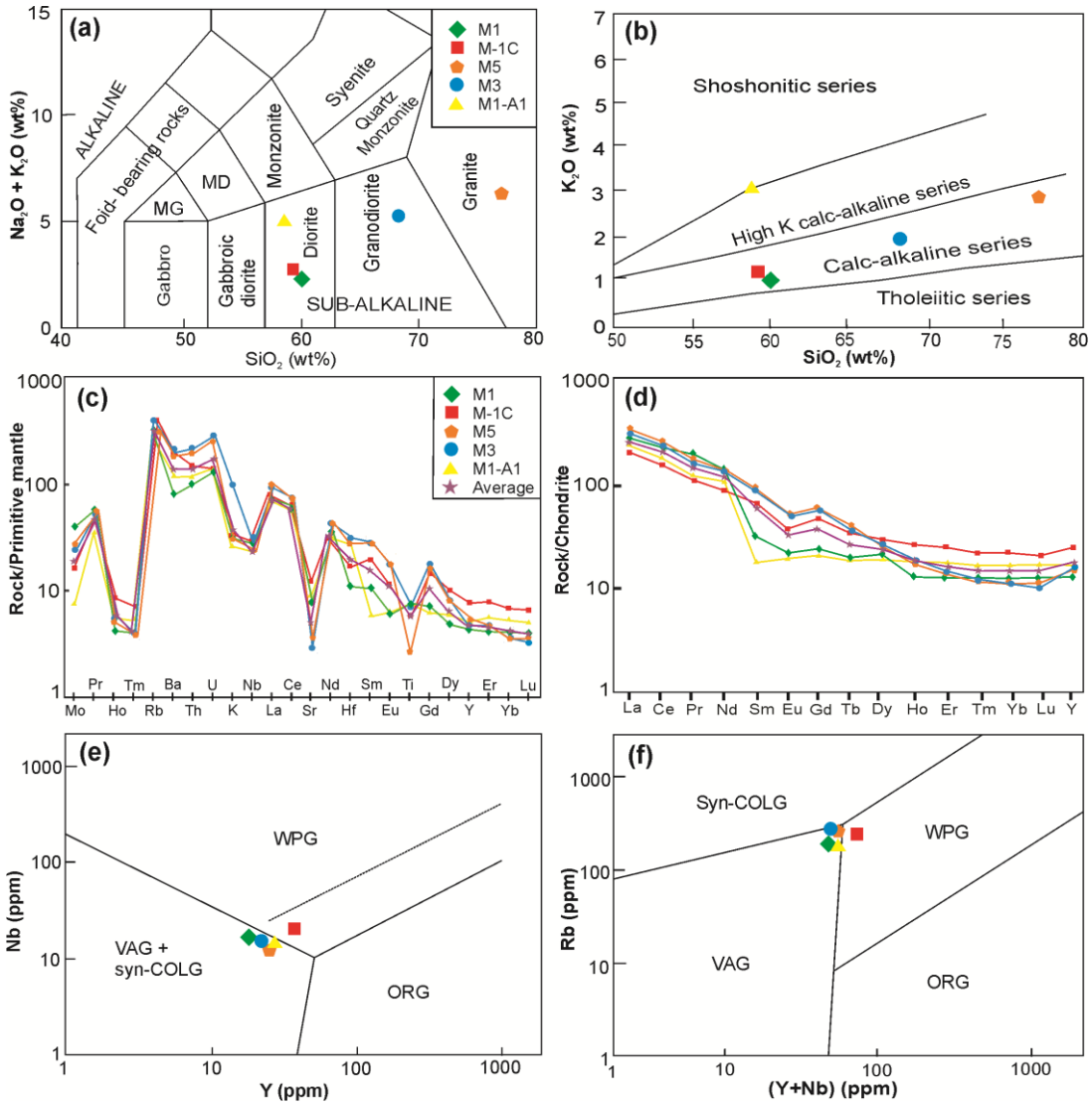

Figure 6.6 (a) Total alkali-silica diagram (Le Maitre et al., 1989),(b) SiO_2 vs K_2O plot, (c) Primitive mantle normalized trace element and Chondrite normalized rare earth elements plot of the Grt-Bt gneisses (Sun and McDonough, 1989), (e) Y vs Nb tectonic discrimination diagram and (f) Y+Nb vs Rb tectonic discrimination diagram; Syn-COLG: syn-collisional granite; WPG: within-plate granite; VAG: volcanic-arc granite; ORG: ocean ridge granite (after Pearce et al.,1984).

6.7.3 Discussion

The TAS diagram for Grt-Bt gneisses displays a contracting protolithic nature varying from diorite, granodiorite, and granite (Fig.6.6a). The granitoids from the BuC also reveal mafic to felsic melt (Rai and Ahmad, 2021). Na and K are highly mobile during metamorphism and hydrothermal alteration; hence, the initial composition of the rock was affected (Deshmukh*et al.*, 2017). The variation of the different major oxides with SiO_2

illustrates a substantial role in the fractionation and crystallization of minerals during the successive evolution of parental magma. The negative anomaly of Nb and Ti for all samples indicates that a subduction tectonic setting has occurred in the BuC. The Grt-Bt gneisses have high SiO_2 and low Cr and Ni concentrations, interpreted as protoliths derived from the hydrous thickened lower crust or may be due to crustal contamination with ascending partial melt. The higher $(La/Yb)_N$ and low HREE contents in Grt-Bt gneisses are signatures of the garnet in the source magma during partial melting (Condie, 2005). The Grt-Bt gneisses have a slight negative Eu anomaly, which indicates the removal of calcic plagioclase from the magma, probably at the initial stage. The Th, La, V, Ce, and Sm enrichment is a likely consequence of the growth of biotite. Differences in the trace elements and REE abundances and variation in the $(La/Lu)_N$ ratio from 95.60 to 266.17 indicate heterogeneous sources and large variation in the degree of partial melting and effect of crustal contamination. The Y vsNb and (Y+Nb) vs Rb tectonic discrimination diagrams (Figs.6.6e&f) show that the protolith of most Grt-Bt gneisses had an affinity towards the volcanic arc granite (VAG), whereas the M-1C sample shows within plate granite (WPG) affinity. This study proposes that the BundelkhandGrt-Bt gneisses are derived mainly from a felsic magma source. This felsic magma is produced by the heat generated during the subduction procedure in the area. A detailed study to determine this tectonic evolution would require more geochemical and geochronological data of various rock types and the *P-T-t* path.

6.8 Amphibolites

6.8.1 Major oxides

A detailed geochemical analysis of two types of amphibolites was performed: garnet-bearing amphibolites (B-6, B-7, B-8, and B-9) and garnet-absent amphibolites (K-1, K-19, B-12, B-10, B-4, and K-10) (Table 6.4). The garnet-bearing amphibolites are compositionally variable in major oxides such as SiO_2 (57.64–77.83 wt%), Al_2O_3 (7.46–16.31 wt%), MgO

(0.47–8.02 wt%), FeO (2.61–13.91 wt%), and also contain lesser amounts of TiO_2 (0.62–1.66 wt%), CaO (1.80–3.51 wt%), and Na_2O (1.03–3.26 wt%). Similarly, garnet-absent amphibolites have also variation in major oxides as; SiO_2 (57.64–77.83 wt%), Al_2O_3 (7.46–16.31 wt%), MgO (0.47–8.02 wt%), FeO (2.61–13.91 wt%), whereas it contains lesser amounts of TiO_2 (0.62–1.66 wt%), CaO (1.80–3.51 wt%), Na_2O (1.03–3.26 wt%). Total alkali versus silica (TAS) plot is used to classify the amphibolites (Le Maitre et al., 1989) (Fig.6.7a); all of the garnet-bearing amphibolites are projected into the basalt region; three garnet-absent amphibolites are projected into the basaltic field, and three are projected into the basaltic andesitic field. Since SiO_2 and alkalies (Na_2O and K_2O) are vulnerable to mobilization during secondary alteration processes such as metasomatism or metamorphism and submarine alteration, immobile trace elements are used to verify them. In this context, all amphibolite samples are plotted in Zr/Ti vsNb/Y (Winchester & Floyd 1977). This diagram reveals that all garnet-bearing amphibolites plot in the basaltic andesite field, and garnet-absent amphibolites plot in the sub-alkaline basalt field (Fig. 6.7b).

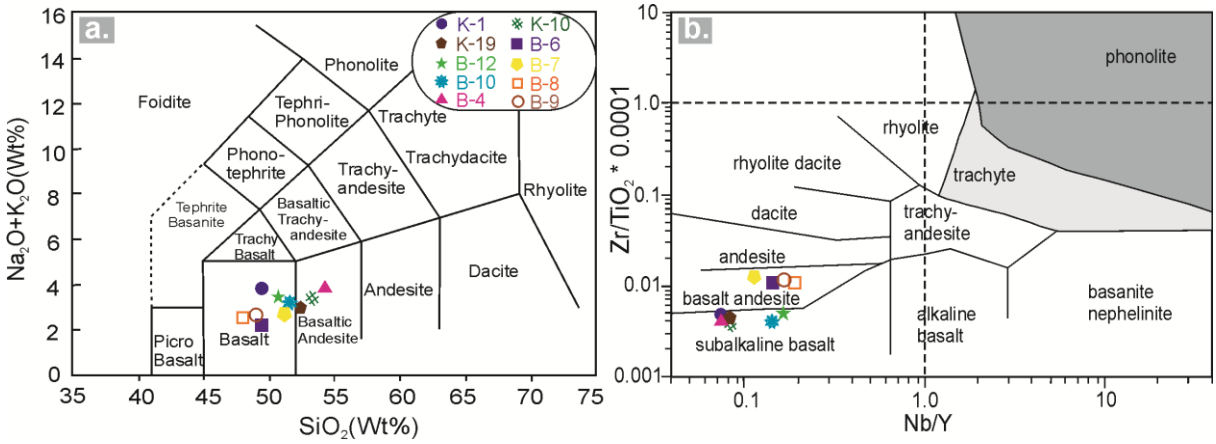

Figure 6.7 (a) Total alkali versus silica (TAS) plot is used to classify the amphibolites (Le Maitre et al., 1989). (b) The Zr/Ti vs Nb/Y plot (Winchester and Floyd 1977).

6.8.2 Trace and REEs

The primitive mantle normalized multi-elemental spider diagram is widely used to determine the nature of trace elements in garnet-bearing and garnet-absent amphibolites, as

well as to constrain their source regions. A subduction orogeny hallmark is an enrichment of large ion lithophile elements (LILE; Th, Rb, Pb, and Y) and the negative anomaly of high field strength elements (HFSE; Nb, Ta, Sr, and Ti), which is observed in the studied amphibolites (Fig. 6.8a). A decrease in Nb and Ti concentrations has validated an island arc setting. Rare earth element (REE) patterns normalized with chondrite for amphibolites are typically organized to define the behaviour of REEs in the studied rocks and to comprehend their source compositions (Fig. 6.8b).

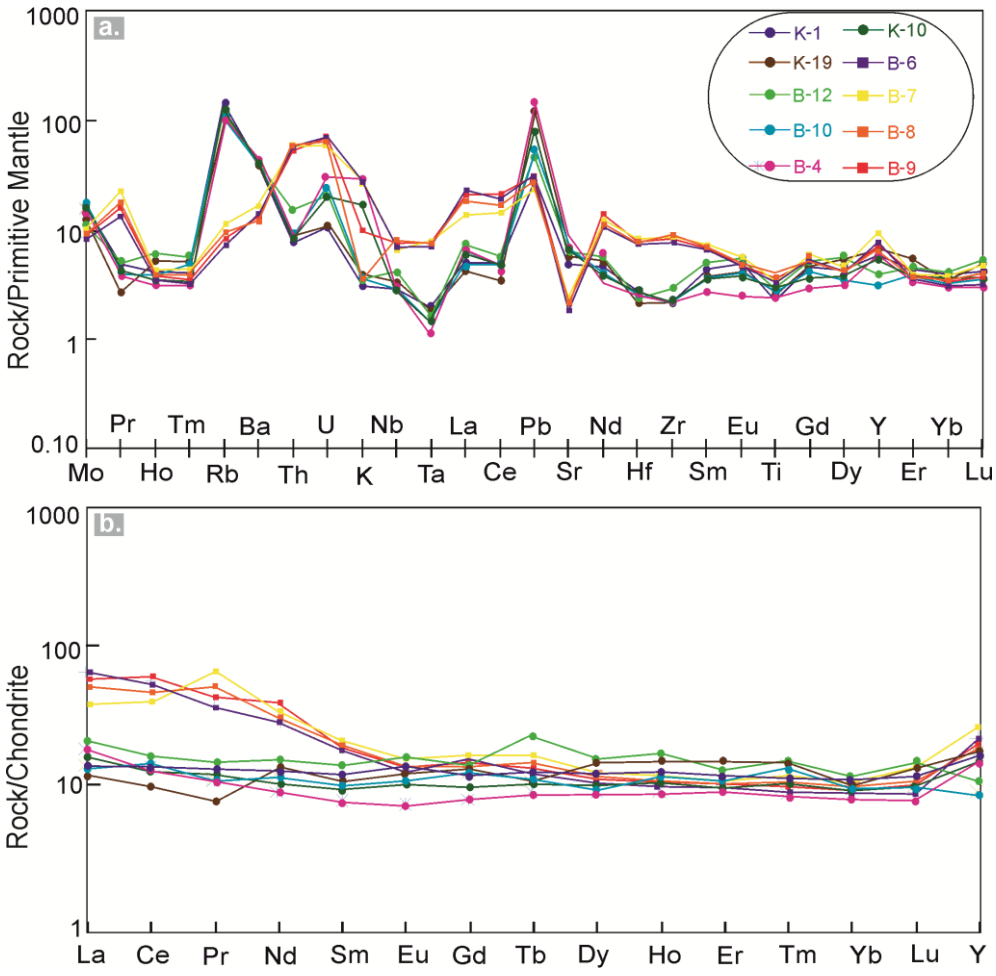

Figure 6.8 (a) Multi-element normalized spider diagram of garnet-bearing as well as garnet-absent amphibolites (normalized after Sun and McDonough, 1989). (b) Chondrite normalized rare earth element plot (normalized after Sun and McDonough, 1989).

Light rare earth element (LREE) enrichment is higher in garnet-bearing amphibolites than heavy rare earth element (HREE) enrichment (La_N/Lu_N = 2.85–7.21), with a little negative Eu anomaly (Eu_N/Eu_{N^*} = 0.76–0.86). However, garnet-absent amphibolites have a

slight enrichment of LREE relative to HREE (La_N/Lu_N = 1.20–2.13) with a slight positive Eu anomaly (Eu_N/Eu_N^* = 1.00–1.13). The sub-parallel REE patterns show that a phase of compositional variation dominated crystal fractionation. Several tectonic discrimination diagrams have been drawn to reveal the protolithic nature of garnet-bearing and garnet-absent amphibolites (Fig. 6.9).

6.8.3 Petrogenesis and tectonic implications

Geochemical data is frequently used to reconstruct the petrogenesis of mantle-derived magmatic rocks. Throughout the Archean, mafic magmatic activity in the form of dykes or intrusions provides a valuable window for observing mantle evolution. More extensive crustal contamination in Archean magma was generated by higher continental geothermal and Th/U compositions of juvenile felsic crust (Abbott et al. 1994). This crustal melt inflow may cause compositional and isotopic changes in primary mantle-derived magma or hybrid magma (Martins et al. 2017), as well as subduction-like indications such as negative Nb, Ta, and Ti anomalies compared to N-MORB, leading to continental intra-plate basalts being misinterpreted as arc basalts (Xia, 2014). The relative diversity of large-ion lithophile elements (LILEs; Rb, Ba, and U) concentration in subduction zones suggests late-stage modifications caused by the action of subduction-resultant fluids (Guilmette et al. 2009). As a consequence, we propose that amphibolites exhibit both spreading and subduction signs, making their tectonic setting difficult to determine. Afterwards, it is critical to look for crustal contamination in amphibolites and determine what role it played in their formation. The studied amphibolites have moderately enriched LREE and LILEs (Ba, Rb, Th, U, and K) but negative Nb, Ta, Zr, and Ti anomalies. Garnet-bearing amphibolites show 4.45–5.04 ppm, and garnet-absent amphibolites have low Th (0.65–1.25 ppm), indicating little crustal contamination or no Th addition in amphibolites (Pearce et al. 2005). Although the BuCamphibolites can be metamorphosed from mafic rocks up to high-grade metamorphism,

their petrogenetic characteristics are accessed by the immobile trace elements such as HFSEs (Ti, Zr, Y and Nb), REEs (La, Sm and Yb) and transition elements (Sc, Y and V) (Mahoney et al. 2000).

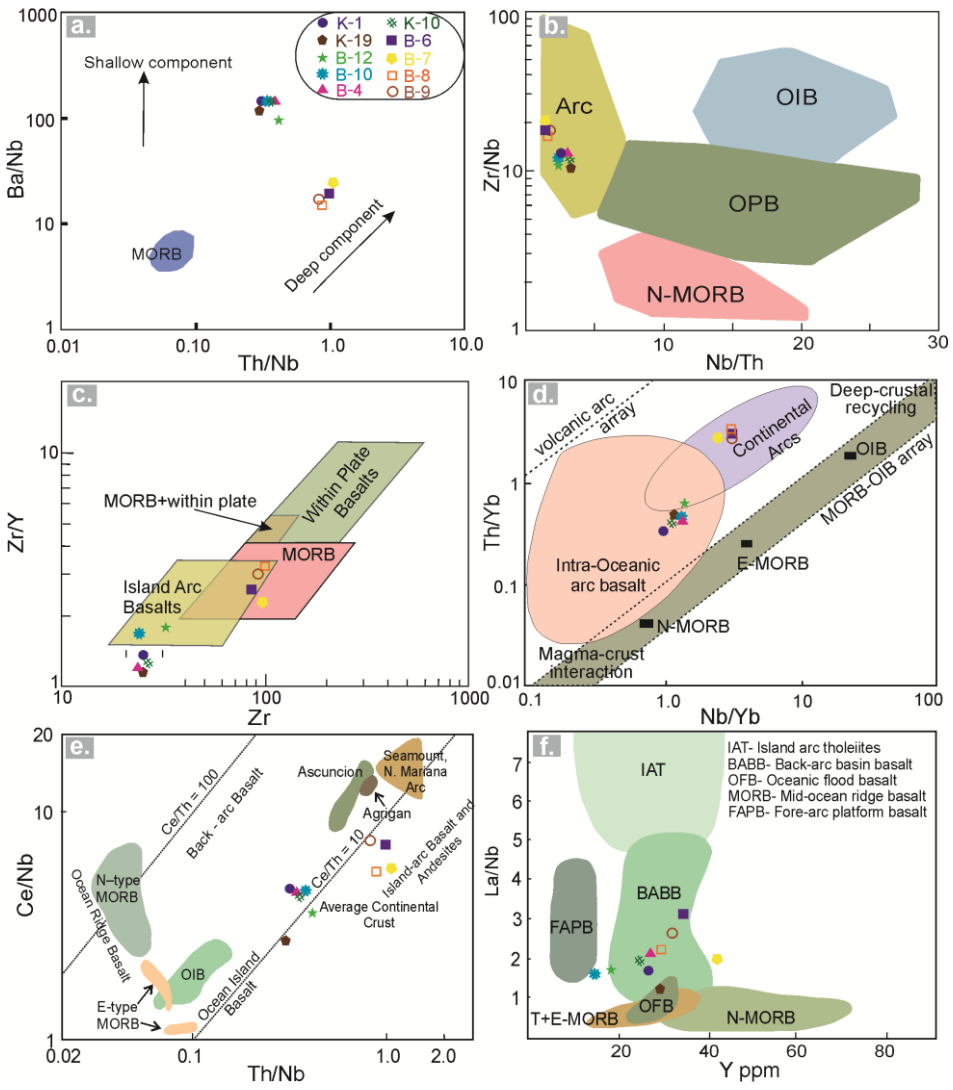

Figure 6.9 (a) Th/Nb vs Ba/Nb diagram (after Pearce and Stern, 2006) showing influence of shallow subduction component in the mantle source for the amphibolites. (b) Nb/Th vs Zr/Nb diagram indicating the arc nature of the amphibolites (after Sun and McDonough, 1989). (c) ZrvsZr/Y diagram showing the island-arc nature of the amphibolites (after Pearce and Norry, 1979). (d) Nb/Yb vs Th/Ybdiagram (Pearce, 2008) depicting a subduction-related enrichment for the Amphibolites samples. Fields for intra-oceanic arc basalt and continental arcs are from Li et al. (2015) and reference therein. (e) Ce/Nb vs Th/Nb plot (after Saunders et al., 1988) showing Island-arc affinity. (f) Y vs La/Nb diagram (after Floyd et al., 1991) showing back-arc affinity,

The tectonic environment is distinguished by HFSE and REE and is linked to the formation of amphibolites. The Th/Nbvs Ba/Nb discrimination diagram (after Pearce &

Stern, 2006) shows a clear influence of the shallow subduction component on garnet-bearing and garnet-absence amphibolites, but no sign of deeper subduction component influence (Fig. 6.9a). The Nb/Th vs Zr/Nb tectonic discrimination diagram suggests an arc-like setting for the amphibolites from the Babina and Mauranipur regions (after Sun & McDonough, 1989, Fig. 6.9b), whereas the Zr vs Zr/Y plot suggests an island arc setting (after Pearce &Norry, 1979, Fig. 6.9c). Furthermore, the concentration of LILEs is nearly identical to the southern BuC metabasalt composition (Hiloidari et al., 2021) and is significantly lower than the Archean Upper Continental Crust (AUCC: Rudnick & Gao, 2004). The subduction-influenced source is also supported by high Th/Yb and low Nb/Yb content; these rock data are located beyond the MORB-OIB array, where garnet-bearing and garnet-absent amphibolites are found in the field of continental arc and intra-oceanic arc basalt, respectively (Fig. 6.9d). According to our findings, the basaltic protolith was formed during orogenic (compressive) tectonism at active margins of island arcs, and their regime was subduction-related. Both amphibolite samples are close to the island basalt setting in the Th/NbvsCe/Nb tectonic discrimination diagram (Saunders et al. 1988: Fig. 6.9e). However, in the Y vs La/Nb diagram (Floyd et al. 1991), both the amphibolites fall in the field of BABB (Fig. 6.9f). This evidence indicates amphibolite generation in a back-arc region during an extensional regime. According to field occurrences of amphibolites and their relationship with host TTGs rocks, geochemical data, and concluded metamorphic records, the protolith of the amphibolites was formed during subduction-related settings in an arc-related setting as enclaves of mafic rocks. These rocks also participated in the Neoarchean collisional tectonism, where amphibolite patches went through pre-peak to peak metamorphism. Meanwhile, these amphibolites interacted with subduction-derived fluids, causing geochemical changes. The amphibolites underwent retrograde metamorphic processes during the exhumation stage.

Table 6.1 Representative major oxides (in wt%), trace elements and REEs (in ppm) compositions of pelitic granulites.

Oxides (wt%)	Grt-Opx-Bt-Sil					Grt-Bt-Sil				
	PM2	**PM1**	**PM3**	**M1-A2**	**M1-A3**	**M1-A4**	**K-2**	**K-3**	**K-4**	**K-5**
SiO_2	57.45	56.81	61.79	55.71	59.82	62.79	66.32	64.56	65.44	62.25
Al_2O_3	19.41	15.23	17.37	17.65	15.8	12.34	19.09	17.58	18.34	17.89
TiO_2	0.96	0.39	0.61	0.8	0.74	0.63	0.67	0.61	0.64	0.72
FeO	10.63	11.10	8.58	9.06	7.54	8.43	7.53	7.10	7.32	8.01
MnO	0.04	0.23	0.04	0.24	0.27	0.07	0.01	0.14	0.08	0.09
MgO	3.19	7.56	4.46	7.26	8.38	7.09	1.50	2.18	1.84	3.4
CaO	1.91	2.97	1.36	2.34	1.67	1.94	1.33	2.75	2.04	2.26
Na_2O	1.22	1.39	1.22	1.74	1.79	1.98	1.26	2.36	1.81	1.32
K_2O	3.67	3.08	3.81	3.9	1.04	3.32	1.86	1.99	1.93	2.68
P_2O_5	0.09	0.37	0.14	0.42	0.68	0.53	0.08	0.27	0.17	0.07
LOI	0.54	0.45	0.27	0.49	0.62	0.5	0.27	0.42	0.34	0.54
TOTAL	99.13	99.58	99.65	99.61	98.35	99.62	99.93	99.95	99.94	99.23
Trace elements and REEs (ppm)										
V	31.21	25.14	34.53	36.26	31.30	33.29	72.06	56.89	64.48	60.68
Co	6.93	5.79	8.64	6.29	5.70	6.75	19.28	17.06	18.17	17.62
Ni	4.29	7.68	8.99	6.54	10.81	8.67	33.8	28	30.90	29.45
Cu	7.22	11.28	7.99	14.37	15.67	19.99	102.8	175	138.90	156.95
Zn	96.85	110.50	114.98	114.40	99.89	93.50	96.8	112.2	104.50	108.35
Rb	202.50	288.67	202.50	299.80	283.50	267.18	125.1	141.8	133.45	137.63
Sr	154.30	198.60	221.67	190.87	167.89	210.34	16	25	20.50	22.75
Zr	162.33	169.00	152.34	177.98	200.00	177.69	201	165.6	183.30	174.45
Nb	7.72	9.88	8.30	11.23	9.67	8.88	7.3	9.7	8.50	9.10
Mo	2.62	2.98	3.67	2.22	3.98	3.85	2.69	3.64	3.17	3.40
Cd	7.78	5.93	8.99	10.22	9.24	8.53	0.12	0.24	0.18	0.21
Ba	582.38	570.34	634.53	492.36	488.89	520.34	569	459	514.00	486.50
Hf	3.62	5.72	9.45	8.34	5.86	9.28	3.62	2.64	3.13	2.89
Ta	0.39	0.46	0.57	0.76	0.67	0.53	0.25	0.3	0.28	0.29
Pb	12.34	17.70	19.80	38.24	23.40	19.28	8.5	17.2	12.85	15.03
Th	18.10	13.61	21.78	19.23	27.24	23.58	28.1	21.59	24.85	23.22
U	2.67	2.28	2.89	3.52	3.09	2.39	2.6	2.78	2.69	2.74
La	54.17	61.67	74.78	56.00	67.19	51.22	90.17	73.57	81.87	86.02
Ce	198.20	112.00	153.49	143.45	117.60	176.53	198	119	158.5	178.25
Pr	22.20	11.70	17.94	14.32	16.41	14.52	22	19.2	20.6	21.30
Nd	56.81	63.04	63.51	52.55	60.94	52.37	81	64.5	72.75	76.88
Sm	9.01	10.56	13.20	9.86	13.35	11.81	14.6	9.4	12	13.30
Eu	1.98	1.45	1.15	1.67	1.29	1.51	1.92	1.41	1.665	1.79
Gd	13.92	9.84	10.21	7.51	12.73	10.84	13.98	8.82	11.4	12.69
Tb	1.63	1.29	1.69	0.96	1.33	1.38	1.65	1.09	1.37	1.51
Dy	7.85	7.63	5.77	4.36	7.30	5.58	7.21	4.63	5.92	6.57
Ho	1.74	1.73	0.80	0.79	1.08	1.23	1.12	1.54	1.33	1.23
Er	2.43	4.64	3.77	2.68	2.98	3.30	2.42	1.64	2.03	2.23
Tm	0.32	0.25	0.43	0.18	0.29	0.35	0.25	0.19	0.22	0.24
Yb	3.12	3.03	2.75	2.87	2.96	3.55	1.31	1.75	1.53	1.42
Lu	0.73	0.53	0.29	0.43	0.65	0.59	0.17	0.38	0.275	0.22
Y	20.22	28.97	36.34	29.14	23.00	28.33	30.08	21.78	25.93	28.01
$(La/Sm)_N$	3.88	3.77	3.66	3.67	3.25	2.80	3.99	5.05	4.40	4.18
$(La/Lu)_N$	7.95	12.47	27.64	13.96	11.08	9.30	56.85	20.75	31.91	41.43
Eu/Eu*	0.54	0.43	0.30	0.59	0.30	0.41	0.41	0.47	0.44	0.42

Table 6.2 Representative major oxides (in wt%), trace elements and REEs (in ppm) compositions of pelitic granulites (continued….).

Oxides	Grt-Bt-Sil		Grt-Opx-Crd-Bt-Sil					
(wt%)	K-6	K-7	M-7	M-8	M-9	M-10	M-1C	M-1D
SiO_2	63.85	65.08	59.56	62.23	58.06	58.29	60.78	61.79
Al_2O_3	18.11	18.60	19.82	15.56	20.90	19.21	18.23	16.37
TiO_2	0.68	0.67	0.72	0.65	0.87	0.82	0.89	0.64
FeO	7.66	7.60	8.67	9.26	10.59	10.22	8.10	8.44
MnO	0.08	0.05	0.05	0.07	0.02	0.04	0.23	0.04
MgO	2.62	2.06	3.59	3.67	2.73	3.46	4.56	5.46
CaO	2.15	1.74	1.12	1.94	1.23	1.88	1.97	1.64
Na_2O	1.57	1.41	1.92	2.21	0.96	1.54	1.39	1.22
K_2O	2.30	2.08	3.33	3.21	3.11	3.62	2.08	3.81
P_2O_5	0.12	0.10	0.09	0.03	0.04	0.09	0.03	0.01
LOI	0.44	0.35	0.51	0.53	0.55	0.54	0.55	0.49
TOTAL	99.59	99.76	99.38	99.36	99.06	99.71	98.81	99.91
Trace elements and REEs (ppm)								
V	68.27	58.79	28.17	29.83	35.39	33.78	32.29	32.25
Co	18.73	17.34	6.36	7.21	7.46	6.00	6.23	6.84
Ni	32.35	28.73	5.99	8.34	7.77	8.68	9.74	6.48
Cu	120.85	165.98	9.25	9.64	11.18	15.02	17.83	13.61
Zn	100.65	110.28	103.68	112.74	114.69	107.15	96.70	95.18
Rb	129.28	139.71	245.59	245.59	251.15	291.65	275.34	234.84
Sr	18.25	23.88	176.45	210.14	206.27	179.38	189.12	182.32
Zr	192.15	170.03	165.67	160.67	165.16	188.99	188.85	170.01
Nb	7.90	9.40	8.80	9.09	9.77	10.45	9.28	8.30
Mo	2.93	3.52	2.80	3.33	2.95	3.10	3.92	3.24
Cd	0.15	0.23	6.86	7.46	9.61	9.73	8.89	8.16
Ba	541.50	472.75	576.36	602.44	563.45	490.63	504.62	551.36
Hf	3.38	2.76	4.67	7.59	8.90	7.10	7.57	6.45
Ta	0.26	0.29	0.43	0.52	0.67	0.72	0.60	0.46
Pb	10.68	16.11	15.02	18.75	29.02	30.82	21.34	15.81
Th	26.47	22.40	15.86	17.70	20.51	23.24	25.41	20.84
U	2.65	2.76	2.48	2.59	3.21	3.31	2.74	2.53
La	83.95	77.72	57.92	68.23	65.39	61.60	59.21	52.70
Ce	168.38	138.75	155.10	132.75	148.47	130.53	147.07	187.37
Pr	20.95	19.90	16.95	14.82	16.13	15.37	15.47	18.36
Nd	74.81	68.63	59.93	63.28	58.03	56.75	56.66	54.59
Sm	12.65	10.70	9.79	11.88	11.53	11.60	12.58	10.41
Eu	1.73	1.54	1.72	1.30	1.41	1.48	1.40	1.74
Gd	12.05	10.11	11.88	10.03	8.86	10.12	11.79	12.38
Tb	1.44	1.23	1.46	1.49	1.33	1.15	1.36	1.51
Dy	6.24	5.28	7.74	6.70	5.07	5.83	6.44	6.72
Ho	1.28	1.44	1.74	1.27	0.80	0.94	1.15	1.48
Er	2.13	1.84	3.54	4.21	3.23	2.83	3.14	2.87
Tm	0.23	0.21	0.28	0.34	0.31	0.24	0.32	0.33
Yb	1.48	1.64	3.08	2.89	2.81	2.92	3.26	3.34
Lu	0.25	0.33	0.63	0.41	0.36	0.54	0.62	0.66
Y	26.97	23.86	24.60	32.66	32.74	26.07	25.67	24.28
$(La/Sm)_N$	4.28	4.69	3.82	3.71	3.66	3.43	3.04	3.27
$(La/Lu)_N$	36.17	25.43	9.85	17.83	19.47	12.22	10.23	8.56
Eu/Eu*	0.43	0.45	0.49	0.36	0.43	0.42	0.35	0.47

Table 6.3 Representative major oxides (in wt%), trace elements and REEs (in ppm) compositions of garnet-biotite gneisses.

Oxides	M1	M-1C	M1-A1	M5	M3
SiO_2	60.09	59.29	57.64	77.83	68.56
Al_2O_3	7.46	10.68	16.31	8.48	9.58
FeO	13.91	11.59	10.15	2.61	7.10
TiO_2	1.66	1.45	1.26	0.62	1.03
MnO	0.26	0.24	0.25	0.04	0.14
MgO	8.02	7.89	5.11	0.47	4.18
CaO	3.51	3.10	1.80	2.40	2.75
Na_2O	1.03	1.45	2.02	3.26	2.36
K_2O	0.99	1.13	3.13	2.85	1.99
P_2O_5	0.65	0.39	0.37	0.14	0.27
LOI	2.20	2.52	1.49	1.01	1.42
Total	99.79	99.73	99.54	99.72	99.37
Na_2O+K_2O	2.03	2.58	5.16	6.11	4.35
A/CNK	1.35	1.88	2.34	1.00	1.44
A/NK	3.68	4.14	3.16	1.39	2.76
K_2O/Na_2O	0.96	0.78	1.55	0.87	0.83
Trace elements (ppm)					
V	30.21	34.14	24.53	35.26	21.28
Cr	24.49	19.47	15.79	10.57	24.12
Mn	378.95	2206.10	1667.72	821.34	736.25
Co	5.94	6.92	7.61	5.26	6.70
Ni	4.34	7.21	8.96	6.68	9.21
Cu	7.11	11.48	7.18	14.17	15.25
Rb	205.69	255.64	202.90	258.63	287.31
Sr	155.94	190.72	211.00	74.23	65.28
Nb	21.34	22.83	19.08	19.58	19.09
Mo	2.69	1.08	0.47	1.74	1.66
Cs	7.85	3.74	0.19	16.65	17.55
K	34.52	35.88	29.88	33.20	99.60
Ba	582.38	1505.54	891.41	1537.53	1429.83
Hf	3.64	5.90	0.47	9.04	10.14
Th	9.16	13.61	1.04	18.68	19.77
U	2.94	3.12	0.20	6.01	6.43
La	56.17	51.57	55.36	73.94	69.30
Ce	128.03	102.31	114.05	141.99	138.51
Pr	16.93	11.64	11.94	16.32	15.41
Nd	56.61	45.80	49.51	64.55	61.94
Sm	5.01	9.56	2.93	13.86	13.35
Eu	1.11	2.18	1.15	3.18	3.02
Gd	4.51	9.36	4.21	11.51	11.73
Tb	0.63	1.29	0.69	1.32	1.33
Dy	4.85	7.82	4.77	6.36	6.30
Ho	0.74	1.50	1.02	0.99	1.02
Er	2.21	4.17	3.06	2.41	2.39
Tm	0.32	0.58	0.43	0.31	0.31
Yb	2.12	3.71	2.94	1.87	1.96
Lu	0.33	0.54	0.42	0.29	0.26
Sc	11.69	22.09	52.01	13.23	11.31
Y	20.72	38.16	26.58	26.19	23.61
∑REE	311.99	312.30	331.08	378.29	361.74
$(La/Sm)_N$	3.89	3.48	1.18	3.44	3.35
$(La/Lu)_N$	172.79	95.60	130.35	259.38	266.17
Eu/Eu*	0.72	0.70	1.00	0.77	0.74

Table 6.4 Representative major oxides (in wt%), trace elements and REEs (in ppm) compositions of garnet bearing and garnet absent amphibolites.

Oxides	Garnet-bearing				Garnet-absent					
(wt%)	B-6	B-7	B-8	B-9	K-1	K-19	B-12	B-10	B-4	K-10
SiO_2	47.65	49.14	46.39	47.27	47.59	50.29	48.94	49.61	52.04	51.17
Al_2O_3	18.64	13.23	17.30	15.76	19.01	17.06	18.04	17.55	12.57	14.82
TiO_2	0.76	0.73	0.87	0.77	0.48	0.57	0.60	0.58	0.54	0.66
FeO	14.14	15.29	14.63	14.96	12.28	11.3	11.79	11.54	13.98	12.64
MnO	0.01	0.17	0.09	0.13	0.27	0.172	0.22	0.20	0.02	0.10
MgO	4.61	6.83	5.69	6.26	4.48	6.56	5.52	6.04	5.92	6.24
CaO	10.02	10.29	10.54	10.42	9.28	8.45	8.86	8.66	8.54	8.50
Na_2O	1.33	2.67	1.99	2.33	3.68	2.85	3.27	3.06	2.85	2.85
K_2O	0.83	0.10	0.46	0.28	0.09	0.12	0.11	0.11	0.88	0.50
P_2O_5	0.08	0.11	0.09	0.10	0.08	0.09	0.09	0.09	0.04	0.07
LOI	1.50	0.98	1.24	1.11	1.40	1.65	1.53	1.59	1.54	1.60
TOTAL	99.58	99.54	99.31	99.39	98.64	99.12	98.95	99.03	98.93	99.13
Trace elements and REEs										
V	135.06	156.27	140.56	137.81	280.69	247.79	232.96	235.52	240.21	260.45
Co	25.97	32.69	26.33	26.15	49.86	31.42	41.38	45.51	39.41	44.63
Ni	86.36	92.35	101.25	93.81	101.72	93.73	111.47	96.58	105.89	103.81
Cu	16.31	11.35	17.45	16.88	7.43	6.39	8.68	6.89	4.87	6.15
Zn	61.02	96.91	78.96	69.99	103.50	132.79	157.44	125.73	135.79	119.64
Rb	4.55	7.14	5.85	5.20	90.20	69.73	75.47	70.40	65.68	77.94
Sr	39.63	50.54	45.08	42.36	104.09	121.39	139.81	155.41	192.50	148.30
Zr	84.71	95.48	98.56	91.63	23.36	24.48	31.86	24.14	24.92	24.14
Nb	5.01	4.69	5.64	5.32	2.01	2.37	2.97	2.05	2.03	2.02
Mo	0.53	0.66	0.59	0.56	1.09	0.79	0.76	0.98	0.95	1.02
Cd	0.10	0.13	0.21	0.16	0.17	0.15	0.18	0.23	0.29	0.23
Ba	95.26	114.58	84.52	89.89	288.67	273.26	279.18	290.15	293.31	290.99
Hf	2.34	2.52	2.43	2.38	0.86	0.67	0.77	0.81	0.77	0.81
Ta	0.30	0.32	0.31	0.31	0.07	0.08	0.07	0.06	0.04	0.06
Pb	5.87	4.22	5.04	5.45	5.13	22.57	9.32	10.24	26.41	15.77
Th	4.98	5.04	5.01	4.45	0.65	0.71	1.25	0.78	0.70	0.68
U	1.48	1.26	1.37	1.42	0.22	0.23	0.44	0.52	0.63	0.42
La	15.73	9.30	12.51	14.12	3.44	2.87	5.12	3.32	4.39	3.91
Ce	34.09	25.15	29.62	37.54	8.63	6.27	10.25	8.88	8.32	8.47
Pr	3.62	6.25	4.93	4.27	1.29	0.74	1.45	1.08	1.07	1.18
Nd	13.67	16.21	14.94	18.41	6.15	6.95	7.54	5.66	4.37	5.26
Sm	2.90	3.25	3.08	2.99	1.92	1.74	2.25	1.58	1.21	1.56
Eu	0.76	0.95	0.86	0.81	0.83	0.73	0.95	0.66	0.43	0.63
Gd	3.22	3.52	2.98	3.10	2.63	2.86	3.02	2.58	1.71	2.17
Tb	0.48	0.65	0.56	0.52	0.47	0.45	0.86	0.42	0.34	0.41
Dy	2.91	3.24	3.08	2.99	3.18	3.88	4.15	2.53	2.36	2.77
Ho	0.59	0.69	0.64	0.62	0.69	0.88	1.01	0.65	0.52	0.61
Er	1.73	1.85	1.79	1.76	2.05	2.57	2.24	1.85	1.54	1.80
Tm	0.24	0.32	0.28	0.26	0.30	0.38	0.41	0.36	0.23	0.26
Yb	1.58	1.85	1.72	1.65	1.99	1.73	2.05	1.68	1.52	1.75
Lu	0.23	0.35	0.29	0.26	0.31	0.35	0.38	0.26	0.22	0.26
Y	34.61	42.15	29.58	32.10	26.72	29.25	18.25	14.56	27.19	24.54
$(La/Sm)_N$	3.50	1.85	2.63	3.05	1.16	1.07	1.47	1.36	2.34	1.62
$(La/Lu)_N$	7.21	2.85	4.59	5.76	1.20	0.88	1.44	1.37	2.13	1.59
Eu/Eu*	0.76	0.86	0.86	0.81	1.13	1.00	1.11	1.00	0.92	1.05